

Acoustic multipath structure in direct zone of deep water and bearing estimation of tow ship noise of towed line array

Zhi-Bin Han(韩志斌), Zhao-Hui Peng (彭朝晖), Jun Song(宋俊), Lei Meng(孟雷), Xiu-Ting Yang(杨秀庭), and Bing Su(苏冰)

Citation: Chin. Phys. B, 2022, 31 (**5**): 054301. DOI: 10.1088/1674-1056/ac364e
Journal homepage: http://cpb.iphy.ac.cn; http://iopscience.iop.org/cpb

What follows is a list of articles you may be interested in

Influence of warm eddies on sound propagation in the Gulf of Mexico

Yao Xiao(肖瑶), Zhenglin Li(李整林), Jun Li(李鋆), Jiaqi Liu(刘佳琪), Karim G Sabra
Chin. Phys. B, 2019, 28 (**5**): 054301. DOI: 10.1088/1674-1056/28/5/054301

Model/data comparison of typhoon-generated noise

Jing-Yan Wang(王璟琰), Feng-Hua Li(李风华)
Chin. Phys. B, 2016, 25 (**12**): 124317. DOI: 10.1088/1674-1056/25/12/124317

Bearing splitting and near-surface source ranging in the direct zone of deep water

Jun-Nan Wu(吴俊楠), Shi-Hong Zhou(周士弘), Zhao-Hui Peng(彭朝晖), Yan Zhang(张岩), Ren-He Zhang(张仁和)
Chin. Phys. B, 2016, 25 (**12**): 124311. DOI: 10.1088/1674-1056/25/12/124311

Spatial correlation of the high intensity zone in deep-water acoustic field

Jun Li(李鋆), Zheng-Lin Li(李整林), Yun Ren(任云)
Chin. Phys. B, 2016, 25 (**12**): 124310. DOI: 10.1088/1674-1056/25/12/124310

Investigation of long-range sound propagation in surface ducts

Duan Rui, Yang Kun-De, Ma Yuan-Liang
Chin. Phys. B, 2013, 22 (**12**): 124301. DOI: 10.1088/1674-1056/22/12/124301

Acoustic multipath structure in direct zone of deep water and bearing estimation of tow ship noise of towed line array

Zhi-Bin Han(韩志斌)[1,†], Zhao-Hui Peng (彭朝晖)[2], Jun Song(宋俊)[1], Lei Meng(孟雷)[1], Xiu-Ting Yang(杨秀庭)[1], and Bing Su(苏冰)[1]

[1] *Unit* 92578 *of PLA, China*

[2] *State Key Laboratory of Acoustics, Institute of Acoustics, Chinese Academy of Sciences, Beijing* 100190, *China*

(Received 12 August 2021; revised manuscript received 2 November 2021; accepted manuscript online 4 November 2021)

In the towed line array sonar system, the tow ship noise is the main factor that affects the sonar performance. Conventional noise cancelling methods assume that the noise is towards the endfire direction of the array. An acoustic experiment employing a towed line array is conducted in the western Pacific Ocean, and a strange bearing-splitting phenomenon of the tow ship noise is observed in the array. The tow ship noise is split into multiple noise signals whose bearings are distributed between 10° and 90° deviating from the endfire direction. The multiple interferences increase the difficulty in recognizing the target for the sonar operator and noise cancellation. Therefore, making the mechanism clear and putting forward the tow ship noise splitting bearing estimation method are imperative. In this paper, the acoustic multi-path structure of the tow ship in deep water is analyzed. Then it is pointed out that the bearing-splitting phenomenon is caused by the main lobe of direct rays and bottom-reflected rays, as well as several side lobes of direct rays. Meanwhile, the indistinguishability between the elevation angle and the bearing angle due to the axial symmetry of a strict horizontal line array causes the bearing to deviate from the endfire direction. Based on the theory above, a method of estimating bearing of the tow ship noise in deep water is proposed. The theoretical analysis results accord with the experimental results, which helps to identify the target and provide correct initial bearing guidance for noise cancelation methods.

Keywords: deep water, direct zone, towed line array, the tow ship noise

PACS: 43.30.Cq, 43.60.Fg, 43.60.Jn **DOI:** 10.1088/1674-1056/ac364e

1. Introduction

The towed line array has advantages of low frequency, large array gain and variable depth, which makes it an effective tool for underwater detection.[1] The tow ship noise is the main factor that affects the sonar performance, which however can be cancelled out through noise cancellation methods. The conventional cancelling methods[2–6] assume that the tow ship noise is towards the endfire direction of the array and adopt different ways to cancel the noises in this direction. However, it was found in the experiment that the direction of the tow ship noise is far from a simple issue of the endfire direction. In the actual environment, the noise of the tow ship can reach the array in multi-path with different elevation angles.[7] The horizontal line array is unable to distinguish between the elevation angle and the bearing angle because of its axial symmetry, which results in the bearing estimation error of the tow ship.[8,9] Hence, the noise from the tow ship can form multiple targets deviating from the endfire direction in the array due to the rays with multi-path and different elevation angles.[10] Meanwhile, the sidelobe of the noise is also strong because the tow ship is very close to the array, which further increases the number of false targets. When the real target and multiple tow ship noise exist in the array at the same time, the accurate locating of the bearings of multiple noises is of critical importance in identifying the target and canceling the noise.

Ma and Liu[5] and Buckingham[6] observed multiple tow ship noise deviating from the endfire direction of the towed line array in the shallow water experiment. Through multipath structure analysis, they suggested that the phenomenon is caused by the rays from the tow ship reflected at least once by the bottom. In deep water, Wu *et al.*[7] analyzed the beam splitting phenomenon specifically when the towed line array observe the target located at a greater distance in the direct zone of deep water. Yang[8] conducted simulations to examine the dependence of the bearing errors with a towed array on the range and bearing of a source at a very large distance. Wu *et al.*[11] analyzed the bearing estimation error and bearing-splitting phenomenon of the deep horizontal array near the seafloor for shallow source.

The above studies in deep water are, in general, for the target at a greater distance in the direct zone. However, an experiment in western Pacific Ocean in the paper shows that the tow ship noise distribution is more complex as the source is much close to the array. It is found that the tow ship noise splits into a number of targets which are distributed in a range between 10° and 90° widely deviating from the endfire direction. The above phenomenon seriously affects target recognition and increases the difficulty in canceling noise. Till now very few literature has focused on the bearing distribution of

[†]Corresponding author. E-mail: 593344287@qq.com

© 2022 Chinese Physical Society and IOP Publishing Ltd

the target in the near field of the direct zone in deep water such as the tow ship noise. In this work, in order to give a theoretical explanation, the acoustic multipath structure in deep water is analyzed, and the results indicate that the tow ship noise reaches the array in the form of the direct ray cluster and the bottom reflection ray cluster. The elevation angle of the direct ray cluster increases significantly outside the mixing layer, which leads the noise bearing to deviate from the endfire direction by a certain angle. In comparison, the elevation angle of the bottom reflection ray cluster is close to vertical direction, with noise bearing being close to the broadside direction in the array. As the energy of the direct ray cluster is much higher than that of the bottom reflection ray cluster, not only the main lobe but also several side lobes of the direct ray cluster can be observed in the array. Therefore, multiple tow ship noise can also be observed in the side lobe directions of the direct ray cluster. Based on the theory above, a method of estimating the direction of the tow ship noise in deep water is proposed. The theoretical results in this paper are consistent with the experimental data, which helps to identify the target and provide correct initial bearing guidance for noise cancellation methods.

2. Towed line array experiment in deep water

In October 2014, an underwater acoustic experiment was conducted in western Pacific Ocean. The sea depth of the experimental area is 5190 m, and the sound speed profile measured is shown in Fig. 1, indicating that there exists a mixture layer of 40 m in thickness. In the experiment, the towed line array was towed by a ship displayed in Fig. 2, showing that the number of the array elements is 192 and the spacing between elements is 1.5 m. The array depth was 140 m and the distance from the array to the tow ship varied between 700 m and 1000 m.

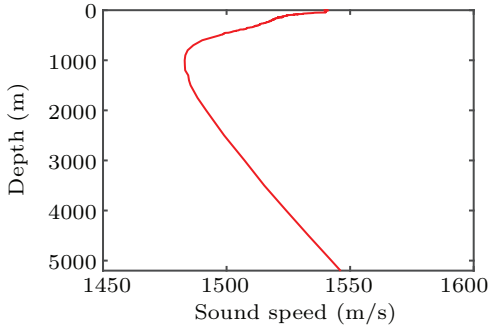


Fig. 1. Sound speed profile measured in experiment.

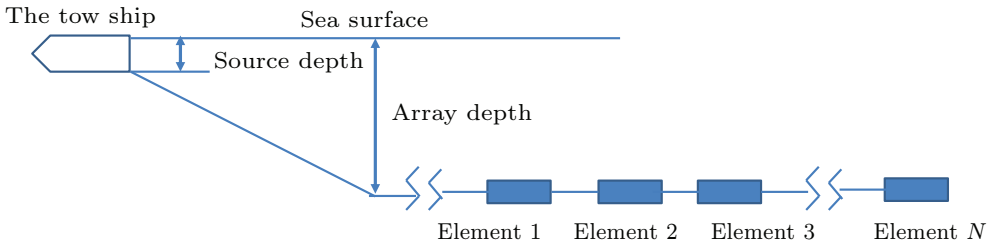


Fig. 2. Diagram of towed line array sonar system.

In a conventional beamforming method, the weight vector $\boldsymbol{W}$ is set to be[12]

$$\boldsymbol{W} = \left[1, \exp\left(\mathrm{j}\frac{\omega s}{c_\mathrm{f}}\sin\theta_\mathrm{c}\right), \ldots, \exp\left(\mathrm{j}\frac{\omega(N-1)s}{c_\mathrm{f}}\sin\theta_\mathrm{c}\right)\right], \quad (1)$$

where N is the number of array elements, s is the spacing between elements. c_f is the reference sound speed normally at the array position, and θ_c is the beamforming scanning angle, ω is the angular frequency and $\omega = 2\pi f$ with f being the source frequency.

Figure 3 shows the bearing-time record (BTR) calculated by the broadband conventional beamforming at 300 Hz–400 Hz. The horizontal axis is the bow bearing, with 0° being the endfire direction and 90° being the broadside direction, while the vertical axis represents the time of flight. The color in the figure changing from blue to yellow indicates the increase of the beam intensity.

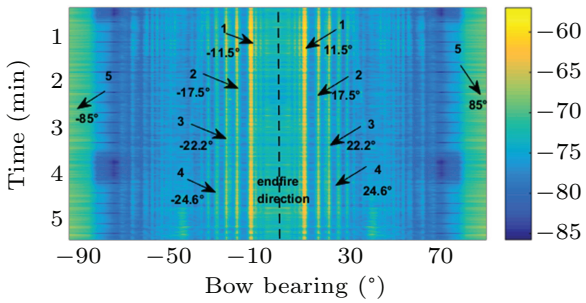


Fig. 3. Beamforming result of array.

As can be seen, first, the bearing estimation error of the tow ship noise is large. The tow ship is located in the endfire direction of the array and the theoretical bow bearing should be 0°. But figure 3 shows that the local maximum value of the BTR of the tow ship noise is at ±11.5°. Second, the tow ship noise distribution is complex. There is an obvious bearing splitting phenomenon that one noise signal splits into a number of signals which are distributed in a range between ±10°

and ±90°, widely deviating from the endfire direction on the BTR. Of all the splitting signals, five can be chosen whose signal intensities are relatively strong, with the strongest values at ±11.5. The split intensity gradually decreases at ±17.5°, ±22.2°, and ±24.6°. Even at ±85° the signal can also be observed. The abolve signals can easily be mistaken for the real target, and thus increasing the difficulty in cancelling noise at the same time.

3. Relationship between bearing estimation result of conventional beamforming and acoustic multipath structure of source

In the actual ocean channel, the directivity function $|Y_0(\theta_{\rm T})|$ of the conventional beamforming method for a horizontal array with N array elements follows the form of Eq. (2)[13] based on the normal mode theory (the derivation process can be seen in Appendix A).

$$|Y_0(\theta_{\rm T})| = \frac{\left|\sum\limits_{m=1}^{M} a_m b_m\right|}{\max\limits_{\theta_{\rm c}}\left|\sum\limits_{m=1}^{M} a_m b_m\right|}, \tag{2}$$

with M being the mode number and $\theta_{\rm T}$ the target bearing that deviates from the broadside direction of the array, a_m and b_m can be obtained from Eqs. (3) and (4) respectively and shown below:

$$a_m = \frac{\rm j}{\rho(z_0)\sqrt{8\pi r}} {\rm e}^{-{\rm j}\frac{\pi}{4}} \psi_m(z_0,\omega)\psi_m(z_r,\omega)\frac{{\rm e}^{{\rm j}\mu_m d_1-\beta_m d_1}}{\sqrt{k_{rm}}}, \tag{3}$$

$$b_m = \sum_{n=1}^{N} {\rm e}^{{\rm j}(n-1)\phi_m} = \frac{\sin(N\phi_m/2)}{\sin(\phi_m/2)} {\rm e}^{{\rm j}\frac{N-1}{2}\phi_m}, \tag{4}$$

where k_{rm} and $\psi_m(z,\omega)$ are the eigenvalue and the eigenfunction of the m-th mode, $k_{rm} = \mu_m + {\rm j}\beta_m$ with μ_m being the horizontal wavenumber and β_m the attenuation cofficient of the m-th mode, z_0 and z_r are the target depth and the array depth respectively, d_1 is the distance from the target to the first element in the array, And ϕ_m can be expressed as

$$\phi_m = \mu_m s\sin\theta_{\rm T} - \frac{\omega s}{c_{\rm f}}\sin\theta_{\rm c}. \tag{5}$$

According to Eq. (2), the directivity function of the array is equivalent to the coherent summation of the directivity functions of the M modes where the directivity function of the n-th mode can be expressed as

$$\begin{aligned} |Y_n(\theta_{\rm T})| &= \frac{|a_n b_n|}{\max\limits_{\theta_{\rm T}}|a_n b_n|} \\ &= \frac{\sin(\frac{N}{2}(\mu_n s\sin\theta_{\rm T} - \frac{\omega s}{c_{\rm f}}\sin\theta_{\rm c}))}{N\sin\left(\frac{1}{2}(\mu_n s\sin\theta_{\rm T} - \frac{\omega s}{c_{\rm f}}\sin\theta_{\rm c})\right)}. \end{aligned} \tag{6}$$

When the n-th normal mode excited by the source plays a dominant role, the main lobe direction $\hat{\theta}_{{\rm T}n}$ can be expressed as

$$\hat{\theta}_{\rm T} = \arcsin\left(\frac{c_{\rm f}\mu_n}{\omega}\sin(\theta_{\rm T})\right) \tag{7}$$

with μ_n is the horizontal wavenumber of the n-th mode.

To clarify the relationship between the beamforming result and the acoustic multi-path structure of source, the ray theory is introduced. According to the equivalence between ray and normal mode,[14–17] the n-th dominant mode whose eigenvalue and horizontal wavenumber are k_r and μ_n corresponding to the dominant ray whose elevation angle is φ_n, which satisfies the following equation:

$$\cos\varphi_n = \left|\frac{\mu_n}{k_r}\right|, \tag{8}$$

where $k_r = \omega/c_{\rm r}$, with $c_{\rm r}$ being the sound speed at the array depth. Substituting Eq. (8) into Eq. (7), $\hat{\theta}_{{\rm T}n}$ can be acquired as follows:

$$\hat{\theta}_{{\rm T}n} = \arcsin\left(\frac{c_{\rm f}\cos\varphi_n}{c_{\rm r}}\sin(\theta_{\rm T})\right). \tag{9}$$

When $c_{\rm f} = c_{\rm r}$, $\hat{\theta}_{{\rm T}n}$ can be expressed as

$$\hat{\theta}_{{\rm T}n} = \arcsin\left(\cos\varphi_n\sin(\theta_{\rm T})\right). \tag{10}$$

It can be seen from Eq. (10) that $\hat{\theta}_{{\rm T}n} = \theta_{\rm T}$ occurs only when $\varphi_n = 0$. When there are several multi-path dominant rays from the source to the array with non-zero elevation angles φ_i, φ_j, …, φ_n, the source with a bearing of $\theta_{\rm T}$ will split into several targets with bearings of $\hat{\theta}_{{\rm T}i}$, $\hat{\theta}_{{\rm T}j}$, …, $\hat{\theta}_{{\rm T}n}$ in the array after conventional beamforming.

4. Analysis of acoustic multipath structure between array and tow ship in deep water

It can be seen from Section 3 that multi-path rays with non-zero elevation angles from the source to the array will lead the bearing to split and deviate as well (see Fig. 3). Therefore, it is necessary to study the vertical arrival structure of the rays from the tow ship to the array in the deep water. Under the sound speed profile in Fig. 1, analysis with bellhop shows that there are 6 propagation paths including direct path (DP), surface-reflected path (SR), bottom-reflected path (BR), surface-bottom-reflected path (SBR), bottom-surface-reflected path (BSR), and surface-bottom-surface-reflected path (SBSR)[18] from the tow ship to the array as shown in Fig. 4. Meanwhile, the arrival times of the 6 rays are shown in Fig. 5.

Considering that the elevation angle is the key factor of bearing splitting and bearing deviation, we divide the rays into two groups according to the elevation angles. Each group contains several rays with similar elevation angles, which form a target at a certain angle deviated from the endfire direction. Two groups will split one target into at least two targets.

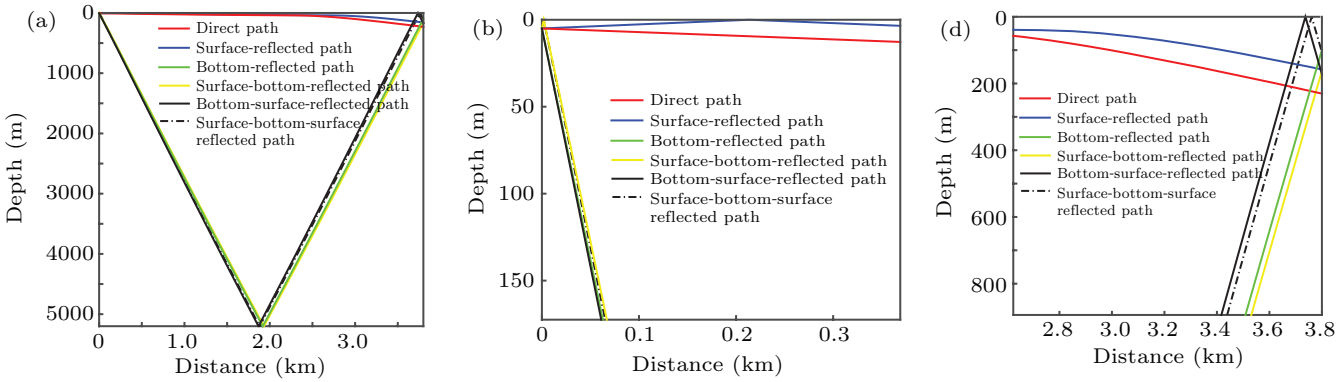


Fig. 4. (a) Paths of 6 rays in direct zone, (b) local enlarged drawing near source, and (c) local enlarged drawing near array.

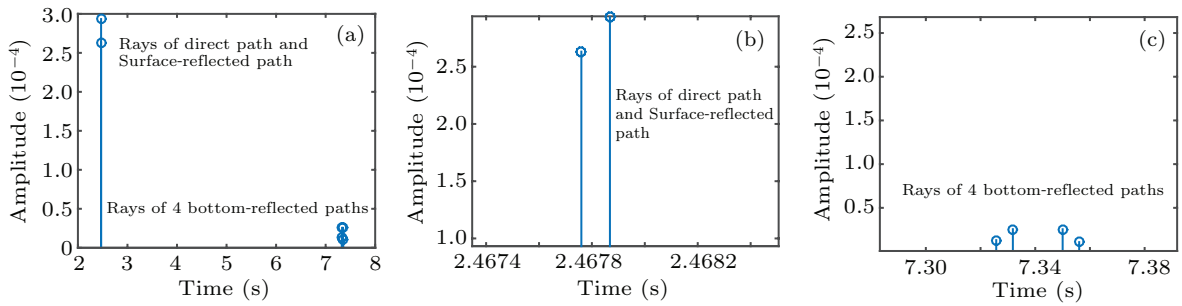


Fig. 5. (a) Arrival times of 6 rays, (b) local enlarged drawing of rays of direct path and surface-reflected path, and (c) local enlarged drawing of rays of 4 bottom-reflected paths.

We call the group containing several rays the ray cluster. According to the definition above, rays of DP and SR have relatively small elevation angles and reach the array first without bottom-reflection. Thus, they are called direct ray cluster for short. In contrast, the rays of BR, SBR, BSR, and SBSR have larger elevation angles than the former and reach the array later through bottom-reflection. Thus, they are called bottom-reflected ray cluster for short. The elevation angles and energy difference between the two ray clusters are studied, which can serve as the theoretical basis for studying the bearing splitting and bearing deviation phenomenon.

Take the average elevation angle of the DP ray and the SR ray as the elevation angle of the direct ray cluster, and the average elevation angle of the BR ray, the SBR ray, the BSR ray, and the SBSR ray as the elevation angle of the bottom-reflected ray cluster, then bellhop is used to calculate the elevation angles of the 2 ray clusters at depths of 0 m–350 m and distances of 0 km–3 km. The result is shown in Fig. 6.

Figure 6 shows that the elevation angles of the direct ray cluster at most of positions are relatively small except for a few positions at very close distances, where only direct rays with large elevation angles can reach. Meanwhile, dramatic changes of the elevation angles exist above and below the mixing layer, with an average value of 2.63° within a depth range of 0 m–40 m and 14° within a depth range of 40 m–350 m. This can be explained by the critical angle theory of the mixing layer, which states that the rays with small emanating angles propagate in the mixing layer and only those with emanating angles greater than the critical angles can reach the array with large depth. On the contrary, the elevation angle of the bottom-reflected ray cluster is large on the whole and the average value reaches 75.29° because rays only with large elevation angles can reach the array through bottom-reflection.

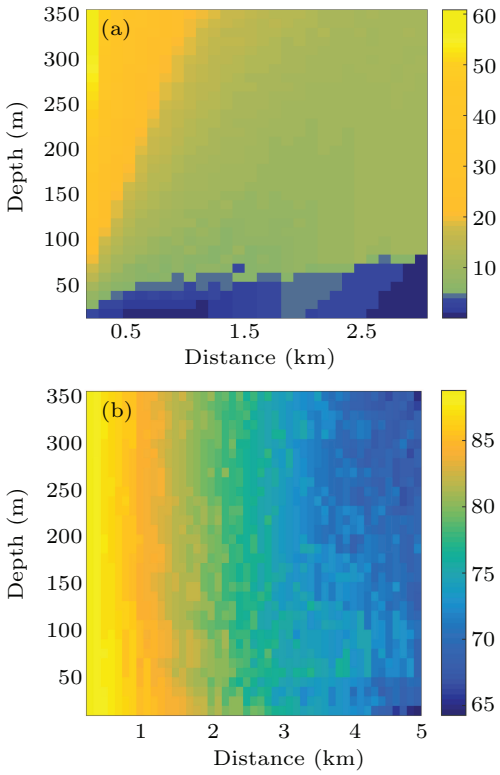


Fig. 6. (a) Elevation angle of direct ray cluster and (b) elevation angle of bottom-reflected ray cluster.

In addition to the angle characteristic, the acoustic energy of the 2 ray clusters is also worth noting, which determines the intensity of the tow ship noise interference on the sonar. Therefore, the ray theory is used to derive the acoustic energy as indicated below.

The pressure $P_{r,z}$ at the coordinate (r,z) can be expressed as the coherent sum of the rays with different paths as follows:[7]

$$P_{r,z} = \sum_{l=1}^{M} \frac{1}{R_l} V_{sl} V_{bl} \, \mathrm{e}^{\mathrm{j}2\pi f t_l(r,z)}, \tag{11}$$

where M is the number of rays, R_l is the path length of the l-th ray, V_{sl} and V_{bl} are the reflection coefficient of the surface and the bottom, respectively, and t_l is the arrival time of the l-th ray from the source to the receiver.

According to Eq. (11), the pressure P_m of the direct ray cluster can be expressed as the coherent sum of the DP ray and the SR ray. Considering that neither of the 2 rays experiences bottom-reflected and the normal of surface reflection coefficient is 1 with phase shift π, P_m can then be written as

$$P_m = \frac{1}{R_1} \mathrm{e}^{\mathrm{j}2\pi f t_1(r,z)} - \frac{1}{R_2} \mathrm{e}^{\mathrm{j}2\pi f t_2(r,z)}, \tag{12}$$

where R_1 and R_2 represent the path length of the DP ray and the SR ray respectively. According to the Lloyd–Mirror effect, equation (12) can be approximated by[19]

$$|P_m| \approx \frac{2}{R} \left| \sin(k z_s \sin\theta) \right|, \tag{13}$$

where z_s is the source depth, R and $\sin\theta$ can be expressed as $\sqrt{r^2+z^2}$ and $z/\sqrt{r^2+z^2}$ respectively.

Similarly, the pressure P_n of the bottom-reflected ray cluster can be expressed as the coherent sum of the BR ray, the SBR ray, the BSR ray, and the SBSR ray. As a result, P_n can be expressed as

$$\begin{aligned} P_n = {} & \frac{1}{R_3} V_{b3} \, \mathrm{e}^{\mathrm{j}2\pi f t_3} - \frac{1}{R_4} V_{b4} \, \mathrm{e}^{\mathrm{j}2\pi f t_4} \\ & - \frac{1}{R_5} V_{b5} \, \mathrm{e}^{\mathrm{j}2\pi f t_5} + \frac{1}{R_6} V_{b6} \, \mathrm{e}^{\mathrm{j}2\pi f t_6}, \end{aligned} \tag{14}$$

where R_3, R_4, R_5, and R_6 are the path length of the BR ray, the BSR ray, the SBR ray, and the SBSR ray respectively; V_{b3}, V_{b4}, V_{b5}, and V_{b6} are the bottom reflection coefficients of 4 rays respectively. After being approximated, equation (14) can be simplified into[20]

$$|P_n| \approx 2 \left| \frac{1}{R_3} V_{b3} \right| \sqrt{1-\cos 2\pi f \Delta t_{12}} \cdot \sqrt{1-\cos 2\pi f \Delta t_{13}}, \tag{15}$$

where Δt_{12} is the difference in time delay between the BR ray and the SBR ray, while Δt_{13} is the difference in time delay between the BR ray and the BSR ray, Δt_{12} and Δt_{13} can be approximated by Eqs. (16) and (17) respectively:

$$\Delta t_{12} = 2 \int_0^{z_s} \sqrt{n^2(z) - \cos^2\varphi} \, \mathrm{d}z / c_0, \tag{16}$$

$$\Delta t_{13} = 2 \int_0^{z_r} \sqrt{n^2(z) - \cos^2\varphi} \, \mathrm{d}z / c_0. \tag{17}$$

Here, $n(z)$ is the index of refraction and φ is the emanating angle of bottom-reflected ray cluster, and c_0 is the sound speed at the source depth. Substituting Eqs. (16) and (17) into Eq. (15) and assuming $n(z)$ to equal 1, $|P_n|$ can be obtained as follows:

$$\begin{aligned} |P_n| &= 4 \left| \frac{1}{R_3} V_{b3} \right| \cdot \left| \sin(\pi f \Delta t_{12}) \right| \cdot \left| \sin(\pi f \Delta t_{13}) \right| \\ &= 4 \left| \frac{1}{R_3} V_{b3} \right| \cdot \left| \sin(2\pi f \cdot z_s \sin\varphi) \right| \\ &\quad \times \left| \sin(2\pi f \cdot z_r \sin\varphi) \right|. \end{aligned} \tag{18}$$

Employing Eqs. (13) and (18) for a source with a frequency of 500 Hz at a depth of 5 m, the values of $|P_m|$ and $|P_n|$ at different depths and distances can be acquired as Fig. 7 if a sound speed profile in Fig. 1 is utilized.

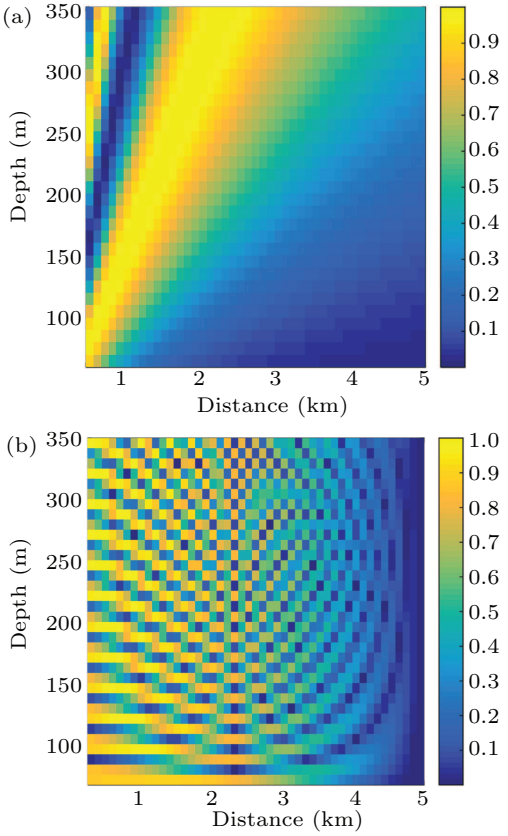


Fig. 7. (a) The $|P_m|$ and (b) $|P_n|$ at different depths and distances.

As can be seen from Fig. 7, $|P_n|$ presents a much more rapid oscillation than $|P_m|$, which can be explained by Eqs. (13) and (18). According to Eq. (18), $|P_n|$ varies with $\sin\varphi$ in two interference cycles of $T_{n1} = 1/fz_s$ and $T_{n2} = 1/fz_r$. Since $T_{n1} \ll 1$ and $T_{n2} \ll 1$, $|P_n|$ changes rapidly when $\sin\varphi$ changes with distance and the depth. In contrast, $|P_m|$ varies with $\sin\theta$ in the interference cycle T_m which can be expressed as

$$T_m = \frac{2\pi}{k z_s} = \frac{c_s}{f z_s}. \tag{19}$$

As $f = 500$ Hz and $z_s = 5$ m are used and $c_s = 1500$, T_m is much bigger than T_{n1} and T_{n2}. Therefore, in this case, $|P_m|$ has a slower oscillation as $\sin\theta$ varies with distance and depth.

Considering the rapid oscillation of $|P_n|$, the local maximum value of $|P_n|$ is chosen as the acoustic intensity which can be expressed as $4\,|(1/R_3)V_{b3}|$. Let $\gamma(r,z)$ be the difference between the acoustic intensity of the direct ray cluster and the bottom-reflected ray cluster, then, according to Eqs. (13) and (18), $\gamma(r,z)$ will be able to be written as

$$\gamma(r,z) = 10\log\frac{R_3^2}{R^2 V_{b3}^2}\,|\sin(kz_s\sin\theta)|^2, \tag{20}$$

where R_3 can be approximated by

$$R_3 \simeq 2\sqrt{\left(\frac{r}{2}\right)^2 + H^2}, \tag{21}$$

with H being the sea depth. Substituting Eq. (21) and $R = \sqrt{r^2+z_r^2}$ into Eq. (20) generates

$$\gamma(r,z) = 10\log\frac{r^2+4H^2}{r^2+z_r^2}\,|\sin(kz_s\sin\theta)|^2 - 10\log V_{b3}^2. \tag{22}$$

Applying the same calculation conditions to Fig. 7 and assuming a bottom loss of 4.5 dB accordance with the bottom loss curves in deep water given by Marsh,[21] the difference in theoretical intensity difference between the 2 clusters can be calculated from Eq. (22), and the results are shown in Fig. 8. Simultaneously, to verify the correctness of Eq. (22), the intensity difference calculated by bellhop at the positions where $|P_n|$ has a local maximum is plotted with the red circles. The two results are basically consistent with each other.

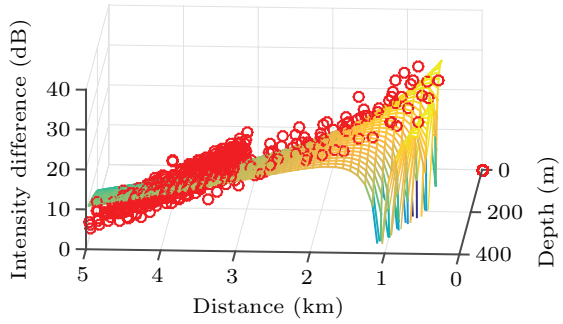


Fig. 8. Plot of difference in intensity between direct ray cluster and bottom-reflected ray cluster *versus* distance.

In Fig. 8, the average intensity difference is 13 dB and the maximum value reaches 30 dB. The large difference is due to the bottom loss and the attenuation in the water of the bottom-reflected ray cluster.

5. Bearing estimation of tow ship noise based on acoustic multipath structure in deep water

It is generally considered that the tow ship noise spreads mainly towards the endfire direction of the array. When a strong signal deviates from the endfire direction, the sonar operator will focus on it and tends to assume it to be a target. Meanwhile, the conventional cancelling methods adopt different ways to cancel the noise in the endfire direction.

But in deep water, the tow ship noise splits into multiple strong signals and distributed in multiple directions deviating from the endfire direction as indicated in Fig. 3. Thus, multiple interferences are formed, which increases the difficulty in recognizing the target for the sonar operator. Meanwhile, some noise cancellation methods are difficult to achieve good results due to the lack of initial bearing guidance.

In order to better identify the target and cancel the noise, in the paper we put forward a method to predict the bearing distribution of the split tow ship noise in deep water, which helps to identify the target and provide correct initial bearing guidance for noise cancellation methods. The method is based on the acoustic multi-path structure analysis above and shown in Fig. 9.

From the method, what is first obtained is the multi-path structure and the elevation angle of the tow ship noise through the bellhop model. Then the strong signal split by the tow ship noise is selected and the bearing of them is calculated. In the selection process, noise formed by both the direct ray cluster and the bottom-reflected ray cluster should be considered. It is worth noting that not only the main lobe of the direct ray cluster but also the side lobe of it can form obvious targets in the towed line array as the energy of the direct ray cluster is high. Thus, all the side lobes of the direct ray cluster with energy greater than the bottom-reflected ray cluster are selected as the strong signal in the method, while the ones with energy less than the bottom-reflected ray cluster are neglected.

To verify the effectiveness of the method and explain the phenomenon in the experiment, we estimate the tow ship noise bearing with the method in Fig. 9, and then compare it with the actual result in Fig. 3. The main process is as follows.

(i) Calculate the elevation angle of the direct ray cluster and that of the bottom-reflected ray cluster irradiated by the tow ship.

The array depth is 140 m, and the distance from the array to the tow ship is 700 m–1000 m. From Fig. 6 it can be seen that the elevation angle of the direct ray cluster and that of the bottom-reflected ray cluster are 11.1°–13.1° and 84.2°–86° respectively.

(ii) Estimate the main lobe bearing of the direct ray cluster and that of the bottom-reflected ray cluster.

The tow ship is towards the endfire direction of the towed array, thus θ_T is 90°. Substituting θ_T into Eq. (10), the bearing estimation result of the tow ship $\hat{\theta}_T$ can be expressed

$$\hat{\theta}_T = \arcsin(\cos\varphi_n). \tag{23}$$

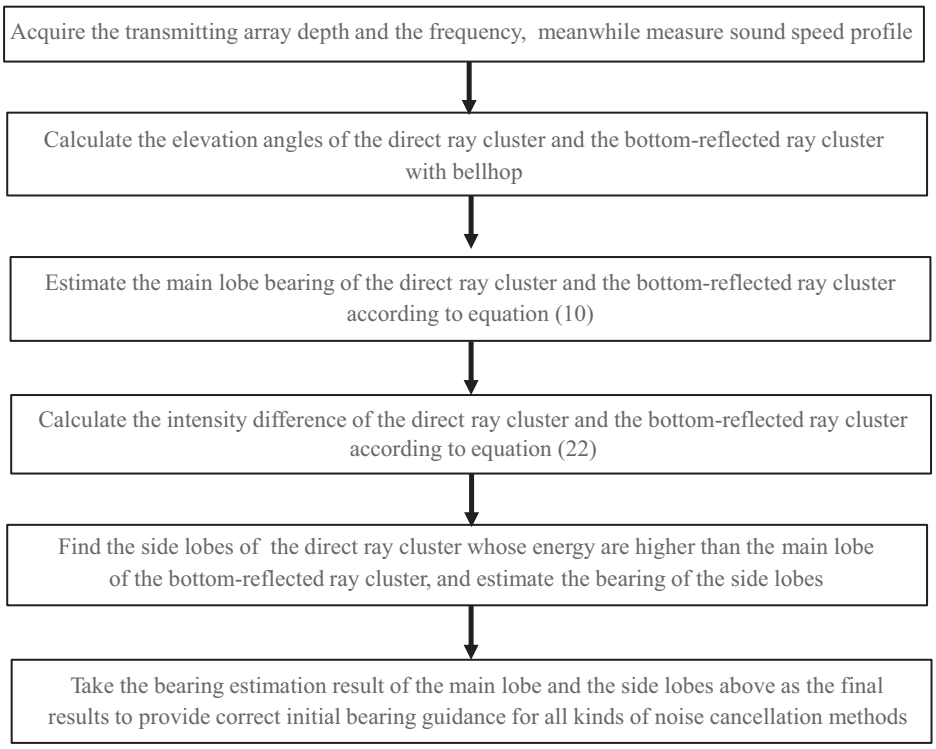


Fig. 9. Main process of bearing estimation method based on acoustic multi-path structure.

Substituting the elevation angle of the direct ray cluster and that of the bottom-reflected ray cluster obtained in step (i) into Eq. (23), the theoretical main lobe bearing of the direct ray cluster and the bottom-reflected ray cluster are 11.1°–13.1° and 84.2°–86° (deviating from the endfire direction) respectively. Meanwhile the actual results in Fig. 3 are 11.5° for target 1 and 85° for target 5, respectively. The theoretical result is basically the same as the actual one.

(iii) Analyze the influence of the sidelobe of the direct ray cluster.

For the array of 192 elements with the element spacing 1.5 m in the experiment, the normalized directivity function is shown in Fig. 10 when $\theta_T = 90°$ and the elevation angle is 0°.

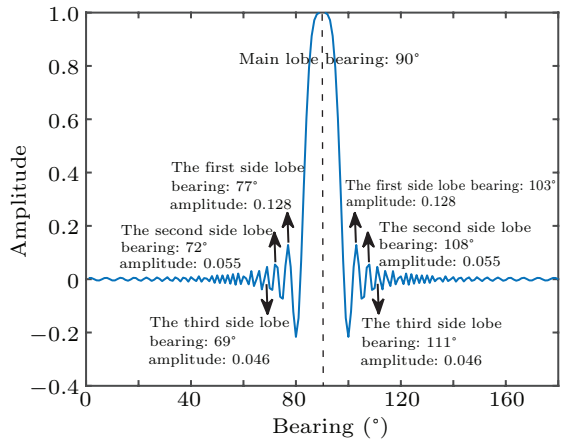


Fig. 10. Normalized directivity function of array with $\theta_T = 90°$ and elevation angle 0°.

According to Fig. 10, the intensity of the main lobe is 17.86 dB, 25.19 dB, and 26.7 dB higher than that of the first side lobe, the second side lobe and the third side lobe respectively. As the acoustic intensity of direct ray clusters is 24.7 dB–26.7 dB higher than that of bottom-reflected ray clusters under the experimental condition, three targets (targets 2–4 in Fig. 3) formed by three side lobes of the direct ray cluster will present a certain angle deviating from the endfire direction, which is consistent with the actual experimental result in Fig. 3.

The actual bearing of the first side lobe, the second side lobe and the third side lobe are 77° (103°), 72° (108°), and 69° (111°) when the elevation angle is 0°. When the actual elevation angle is 11.1°–13.1° under the experimental condition, the bearing estimation results of the first sidelobe, the second sidelobe and the third sidelobe are 71.57°–73.35° (106.65°–108.43°), 67.8°–69.25° (110.75°–112.2°), and 65.37°–66.63° (113.37°–114.63°), respectively, according to Eq. (10). Meanwhile, the actual experimental results in Fig. 3 are 72.5° (107.5°, target 2), 68° (112°, target 3), and 65.4° (114.6°, target 4), which are basically the same as the estimation results.

6. Conclusions

The tow ship noise is the main factor that affects the towed line array performance. It is generally considered that the tow ship noise is towards the endfire direction of the towed array. Therefore, different kinds of noise cancellation methods are used to cancel the tow ship noise towards the endfire direction. But in deep water, the tow ship noise deviates from the

endfire direction and spreads in multiple bearings because of the rays with multi-path and different elevation angles. How to accurately estimate the bearings of the tow ship noise and how to provide initial bearing guidance for all kinds of noise cancellation methods have become a key problem. In this paper, the acoustic multipath structure between the array and the tow ship in deep water is analyzed. Based on the analysis results, a bearing estimation method of tow ship noise in deep water is proposed. After that, the validity of the method is verified in experiment. The main conclusions are as follows.

(I) The towed line array is usually located in the direct zone of the tow ship noise in deep water. The tow ship noise reaches the array in the form of the direct ray cluster and bottom-reflected ray cluster. The former includes the rays of DP and SR which have relatively small elevation angles; the latter includes the rays of BR, SBR, BSR, and SBSR which have large elevation angles.

(II) When the array depth is beyond the mixing layer, the elevation angle of the direct ray cluster increases significantly. As a result, the bearing estimation result of the direct ray cluster deviates from the endfire direction. In comparison, the elevation angle of the bottom-reflected ray cluster is nearly vertical, which makes the bearing estimation result approach to the broadside direction.

(III) The energy of several side lobes of the direct ray cluster is higher than that of the main lobe of the bottom-reflected ray cluster. Therefore, multiple targets will appear, caused by the side lobes of the direct ray cluster.

(IV) Aiming at the bearing splitting phenomenon of tow ship noise in the array, we can estimate the amount and the bearing of the multi-path noise by analyzing the elevation angles and the energy of the direct ray cluster and the reflected ray cluster.

After that, the initial orientation guidance can be provided for various noise cancellation methods.

Acknowledgements

Project supported by the National Defense Basic Science Research Program, China (Grant No. JCKY2016607C009) and the Youth Innovation Promotion Association of the Chinese Academy of Sciences (Grant No. 2018025).

Appendix A

For a towed lined array sonar with N array elements, the received signal vector $\boldsymbol{X}(\omega)$ can be expressed as

$$\begin{aligned}\boldsymbol{X}(\omega) &= [x_1(\omega), x_2(\omega), \ldots, x_n(\omega), \ldots, x_N(\omega)]^{\mathrm{T}} \\ &= s(\omega)\cdot\boldsymbol{P}(\omega) + \boldsymbol{N}(\omega),\end{aligned} \tag{A1}$$

where $x_n(\omega)$ is the received signal of the n-th array element, N the element number, $s(\omega)$ the signal spectrum, $\boldsymbol{N}(\omega)$ the noise spectrum vector, and $\boldsymbol{P}(\omega)$ the channel transfer function vector and can be expressed as

$$\boldsymbol{P}(\omega) = [p_1(\omega), p_2(\omega)\ldots, p_n(\omega)\ldots, p_N(\omega)]^{\mathrm{T}}, \tag{A2}$$

with $p_n(\omega)$ being the channel transfer function of the n-th array element which can be written as[22]

$$\begin{aligned}p_n(\omega) = &\frac{j}{\rho(z_0)\sqrt{8\pi r}}\exp\left(-\mathrm{j}\frac{\pi}{4}\right) \\ &\times\sum_M \psi_m(z_0,\omega)\psi_m(z_r,\omega)\frac{\mathrm{e}^{\mathrm{j}\mu_m d_n-\beta_m d_n}}{\sqrt{k_{rm}}}.\end{aligned} \tag{A3}$$

Here, k_{rm} and $\psi_m(z,\omega)$ are the eigenvalue and the eigenfunction of the m-th mode, $k_{rm}=\mu_m+\mathrm{j}\beta_m$ with μ_m and β_m being the horizontal wavenumber and the attenuation cofficient of the m-th mode respectively; z_0 and z_r are the target depth and the array depth, respectively; d_n is the distance from the target to the n-th element in the array.

When using conventional beamforming method with weight vector $\boldsymbol{W}$ in Eq. (1), the output power $P_{\mathrm{out}}(\omega)$ can be written as

$$\begin{aligned}P_{\mathrm{out}}(\omega) &= \left|\sum_{n=1}^{N} w_n^* x_n(\omega)\right|^2 \\ &= \boldsymbol{W}^{\boldsymbol{H}}(\omega)\boldsymbol{X}(\omega)\boldsymbol{X}^{\boldsymbol{H}}(\omega)\boldsymbol{W}(\omega),\end{aligned} \tag{A4}$$

where the superscript $*$ denotes the complex conjugate. Substituting Eq. (A1) and Eq. (1) into Eq. (A4) generates

$$P_{\mathrm{out}}(\omega) = \delta_{\mathrm{s}}^2\left|\sum_{m=1}^{M} a_m b_m\right|^2 + N\delta_n^2, \tag{A5}$$

where δ_{s}^2 and δ_n^2 are the power spectral density of the source and the noise respectively, a_m represents the amplitude term and b_m denotes the phase term, which can be written as

$$\begin{aligned}a_m = &\frac{\mathrm{j}}{\rho(z_0)\sqrt{8\pi r}}\exp\left(-\mathrm{j}\frac{\pi}{4}\right)\psi_m(z_0,\omega)\psi_m(z_r,\omega) \\ &\times\frac{\mathrm{e}^{\mathrm{j}\mu_m d_1-\beta_m d_1}}{\sqrt{k_{rm}}},\end{aligned} \tag{A6}$$

$$\begin{aligned}b_m &= \sum_{n=1}^{N}\mathrm{e}^{\mathrm{j}(n-1)\phi_m} = \frac{1-\mathrm{e}^{\mathrm{j}N\phi_m}}{1-\mathrm{e}^{\mathrm{j}\phi_m}} \\ &= \frac{\sin(N\phi_m/2)}{\sin(\phi_m/2)}\exp\left\{\mathrm{j}\frac{N-1}{2}\phi_m\right\},\end{aligned} \tag{A7}$$

where $\phi_m=\mu_m s\sin\theta_{\mathrm{T}}-(\omega s/c_{\mathrm{f}})\sin\theta_{\mathrm{c}}$ with θ_{T} being the target bearing (the angle deviating from array broadside direction).

According to Eq. (A5), the directivity function $|Y_0(\theta_{\mathrm{T}})|$ of the array in actual ocean channel can be expressed as

$$|Y_0(\theta_{\mathrm{T}})| = \frac{\left|\sum\limits_{m=1}^{M} a_m b_m\right|}{\max\limits_{\theta_{\mathrm{T}}}\left|\sum\limits_{m=1}^{M} a_m b_m\right|}. \tag{A8}$$

References

[1] Groen J 2005 *IEEE Journal of Oceanic Engineering* **30** 348
[2] Godara and Lal C 1989 *J. Acoust. Soc. Am.* **85** 202
[3] Robert M K and Beerens S P 2002 *Conference Proceedings UDT Europe*, June 18–21, 2002, Spezia, Italy, p. 614
[4] Liu B Q and Du X M 2007 *National Academic Conference on underwater acoustic*, October 12, 2007, Zhengzhou, China, p. 154
[5] Ma Y L and Liu M A 2003 *Chin. J. Acoust.* **22** 10
[6] Buckingham M J 1984 *IEE Prceedings* **131** 298
[7] Wu J N, Zhou S H, Peng Z H, Zhang Y and Zhang R H 2016 *Chin. Phys. B* **25** 124311
[8] Yang T C 2003 *J. Acoust. Soc. Am.* **113** 1342
[9] Han Z B, Peng Z H and Liu Y 2019 *J. Appl. Acoust.* **38** 569
[10] Wu J N, Zhou S H and Zhang Y 2016 *Sci. Sin. Phys. Mech. Astron.* **46** 76
[11] Wu Y Q, Zhang W, Hu Z L, *et al.* 2021 *Acoustics Australia*
[12] Xie L, Sun C, Liu X H, Jiang G Y 2016 *Acta Phys. Sin.* **65** 144303 (in Chinese)
[13] Song J 2005 *Underwater acoustical problems of large-aperture line fiber optic hydrophone array* Ph. D. Dissertation (Changsha: National University of Defense Technology) (in Chinese)
[14] Tindle C T and Guthrie K M 1974 *J. Sound Vib.* **34** 291
[15] Kamel A and Felsen L B 1982 *J. Acoust. Soc. Am.* **71** 1445
[16] Lin J, Zhao Y, Wang H and Chen P 2015 *J. Nanjing Univ. Nat. Sci.* **51** 1223
[17] Han Z B, Peng Z H and Liu X H 2020 *Acta Phys. Sin.* **69** 114301 (in Chinese)
[18] Weng J B, Li F H and Guo Y G 2016 *Acta Acustica* **41** 330
[19] Finn B J, William A K, Michael B P and Henrik S *Computational Ocean Acoustics* (New York: AIP Press) pp. 14–16
[20] Weng J B and Yang Y M 2018 *Acta Acustica* **43** 905
[21] Marsh H W 1978 *J. Acoust. Soc. Am.* **36** 2003
[22] Guo X L, Yang K D, Ma Y L and Yang Q L 2016 *Acta Phys. Sin.* **65** 214302 (in Chinese)